The Thesis Committee for Jeremy Arkin
Certifies that this is the approved version of the following thesis:

Investigation into Optimizing Laser Speckle Contrast Imaging Illumination

APPROVED BY
SUPERVISING COMMITTEE:

Supervisor:

Andrew K. Dunn

Thomas Milner

Investigation into Optimizing Laser Speckle Contrast Imaging Illumination

by

Jeremy Sandon Arkin, B.E.

Thesis

Presented to the Faculty of the Graduate School of

The University of Texas at Austin

in Partial Fulfillment

of the Requirements

for the Degree of

Master of Science in Engineering

The University of Texas at Austin

May 2017

Acknowledgements

I would like to give a special thank my advisor Dr. Andrew Dunn for his support and guidance throughout my two years. A big thank you to Dr. Lisa Richards, Colin Sullender, and Dr. Shams Kazmi for always answering my incessant questions, engaging me in discussion, and all your assistance during experiments. To my family, thank you for your constant love and support. I would not be where I am without you and am so fortunate to have you in my corner as well as providing me the opportunity to pursue my goals.

Abstract

Investigation into Optimizing Laser Speckle Contrast Imaging Illumination

Jeremy Sandon Arkin, M.S.E.

The University of Texas at Austin, 2017

Supervisor: Andrew K. Dunn

The primary purpose of this work is to optimize the illumination parameters used for laser speckle imaging and investigate how spatial modulation of the light used for illumination can enhance the sampling volume. An in-line illumination scheme is detailed that removes the need to manually position a side mounted coherent light source, instead utilizing a polarizing beam splitter (PBS) and linear polarizer to illuminate the sample plane through the same objective used to collect the backscattered light. This method ensures repeated, robust interrogation of the sample plane and allows for control over the light intensity using the polarizing elements.

Spatial modulation of the illumination beam was then investigated as a method to increase the depth-penetration of LSCI. The premise was to use a focused beam of light, as opposed to a traditional wide-field beam, and illuminate the sample at various distances from the detector increasing the probability scattered photons sample deeper volumes. Single and two-point source configurations were used to image a microfluidic phantom with added static scattering layers to simulate different vessel depths. Varying

the distance between the source and the detector, the camera field of view (FOV), we showed that it is possible to collect information from submerged vessels using a non-full field approach. This led to the design and implementation of an in-line, DMD-based illumination scheme that allows the projection and modulation of spatially complex illumination schemes.

Table of Contents

List of Figures

Chapter 1: Introduction

The human body relies on blood for the transport of oxygen, nutrients, and metabolic waste, as well as other molecules required for signaling and fighting foreign bodies. Oxygen and nutrients enable cellular metabolism, providing energy for cells to work together in complex systems to execute specific functions. Groupings of specialized cells form tissues that function together to create organs. Depending on the tissue or organ function, the circulatory system must ensure that certain energy requirements are met by supplying oxygenated blood in order to execute these functions. In general, the amount of blood supplied by the circulatory system to various areas of the body is indicative of their specific energy demands. Therefore, the study of dynamic blood flow is critical to understanding the metabolic needs of tissue throughout the body as well as processes and safeguards which are in place to ensure the vitality of cells.

Many techniques have been developed to study the dynamics of blood flow. Laser-Doppler Flowmetry (LDF) has traditionally been used to image cerebral blood flow by collecting blood flow information at a series of individual points[1]. LDF uses coherent light to illuminate tissue and then analyzes the frequency spectrum of back-scattered photons that interacted with moving particles. Scanning techniques can be used to collect LDF point measurements across the entire region of interest generating a spatially-resolved flow map, known as Laser Doppler Imaging (LDI)[23]. The drawback to LDI is that it has limited temporal resolution due to the time and processing required to scan and process an entire region of interest.

Laser speckle contrast imagine (LSCI) is another technique used to generate spatially resolved flow maps based on the same dynamic-light scattering (DLS)

principles as LDI. LSCI was first introduced by Fercher and Briers over three decades ago and since been used for a host of flow-imaging applications[4]. While LSCI has most commonly been used to image blood flow in the brain, it has proven its versatility as an imaging modality for acquiring blood flow information in skin, retina, and other tissues[5,6,7]. LSCI offers significant advantages over other imaging techniques as it is inherently full field and requires no exogenous agents. Since LSCI is based on DLS, it is inherently limited in its ability to acquire depth resolved flow information. There are various clinical scenarios that could benefit from depth resolved flow information such as imaging the reperfusion of tissue following a skin graph or imaging intricate vasculature arrangements in the cortex of the brain following a stroke.

SECTION 1: FULL FIELD

Chapter 2: In-Line Illumination

2.1 SPECKLE BACKGROUND / CALCULATION

Laser speckle is a random interference pattern that is generated when coherent light interacts with a random scattering medium. Photons incident on the scattering medium undergo multiple scattering events as they interact with particles in the medium before exiting and traveling to a detector. The detector captures a 2D random intensity pattern that appears to have a granular, "speckle" pattern corresponding to bright spots of constructive interference, and dark spots of destructive interference. If the medium contains moving particles, scattering caused from these particles will result in fluctuations in the speckle pattern in time and space. Analyzing the temporal or spatial fluctuations of the speckle pattern can provide quantitative information about the motion of these scattering particles [48]. Rapid intensity fluctuations, caused by areas with large degrees of motion, result in blurring of the speckle pattern. The blurring is actually decorrelation of the speckle pattern where fast moving scatters decorrelate the pattern to a greater extent than slow moving scatters. To quantify the spatial degree of blurring, the speckle contrast is calculated, which is the ratio of the standard deviation to the mean of the local intensity[9].

$$K_s = \frac{\sigma_s}{\langle I \rangle} \quad (1)$$

An image of the speckle pattern can be converted to a speckle contrast image by calculating this ratio at every pixel in the image from the surrounding NxN pixel region and sliding this window across the entire image as shown below in Figure 1[5].

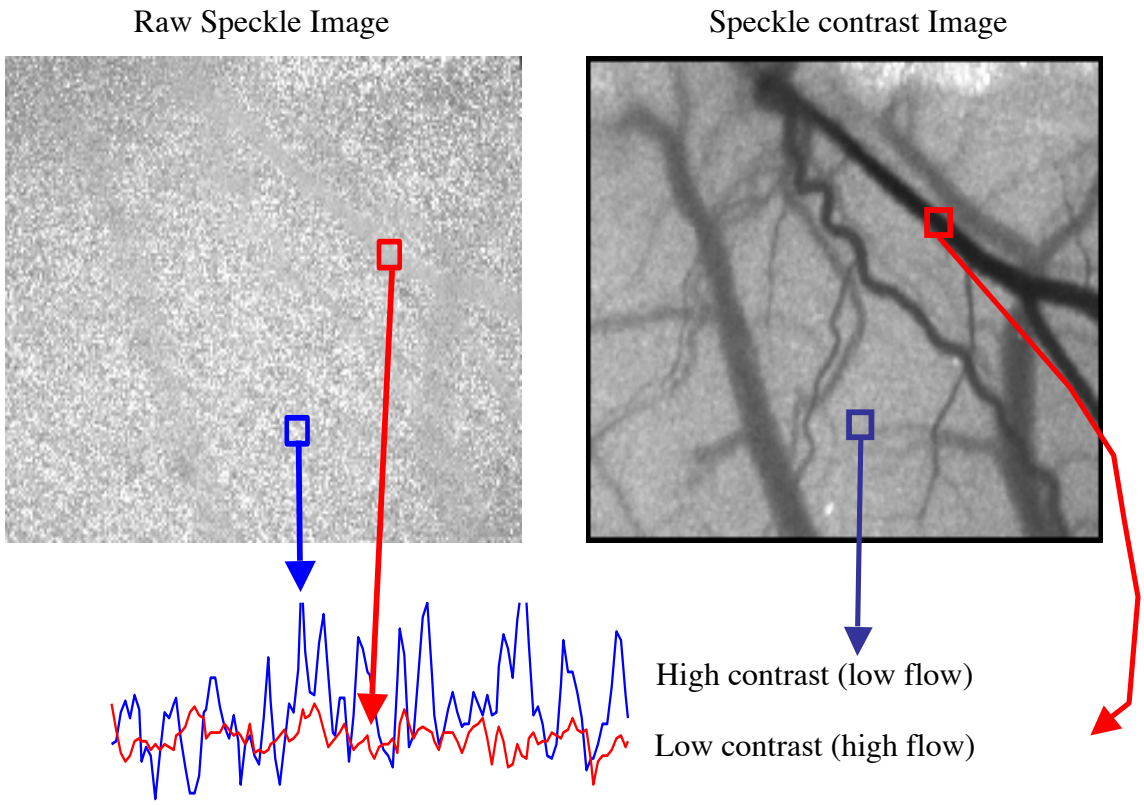

Figure 1: Raw image and computed speckle contrast image. In regions of high flow, the speckles blur, decreasing the contrast in such regions whereas in regions of relatively low flow, there is higher contrast.

The window must be selected to be large enough to accurately determine the mean and the standard deviation. Window sizes of 3x3, 5x5, and 7x7 are typically used for computing the speckle contrast image. The window dimension must be an odd number as the result is applied to the center pixel of the window and then slid over to the next pixel. Sliding of the NxN window across a raw image, like the one shown on the left in Figure 1, generates a speckle contrast image shown on the right which is a spatially resolved flow map. The box in red indicates a region of fast moving scatters that has low contrast indicative of high flow. Fast flows reduce the variance seen in the local speckle

pattern, which decreases the speckle contrast according to Equation 1. Areas of little to no flow, indicated by the box in the blue, have high variance and therefore speckle contrast values closer to 1.

2.2 In-Line Illumination

LSCI uses a coherent light source that is conventionally mounted separately of the detector, and angled such that the sample located beneath the detector is adequately illuminated as shown below in Figure 2.

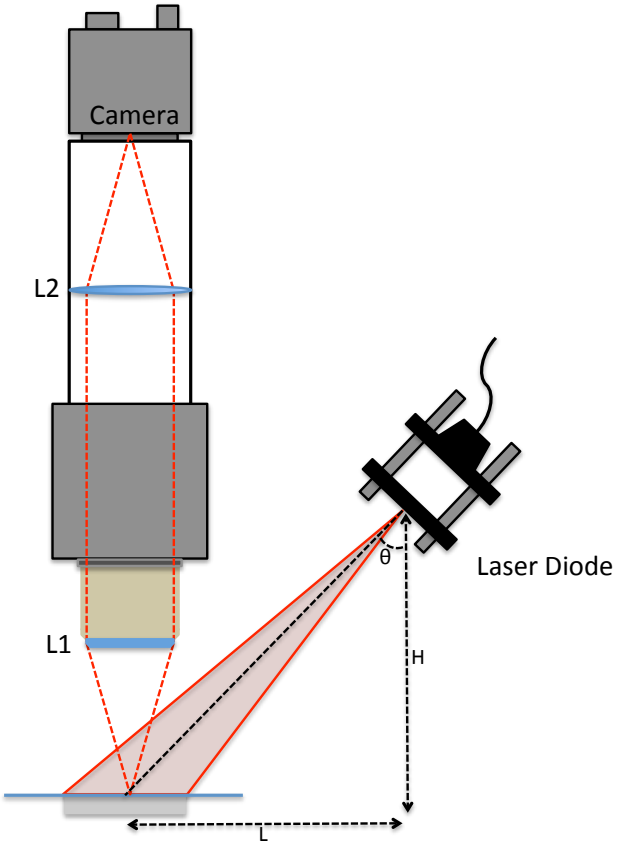

Figure 2: Schematic of conventional side illumination laser speckle system.

In the positioning of the laser, one must ensure the light levels are sufficient which is typically done through moving and or angling the beam. It is important that the

beam evenly illuminates the field of view and there are no irregular patterns or spots with significantly different intensities. The final check is to qualitatively examine the speckles themselves, which should appear crisp and grainy. For someone who works in our lab and has experience with LSCI, this process is often quick and intuitive. In consulting with other groups who seek our assistance in designing and building their own laser speckle system, we realized this process of properly positioning the laser to meet the necessary criteria required of laser speckle may not be as straightforward. Similarly, if we were to describe an experimental setup to another group trying to recreate a setup, while they could buy the same pieces, position the detector the same distance from the sample, and so on, proper positioning of the illumination source such that the angle, distance, spread of light, and position on the sample were identical, would be nearly impossible.

This prompted us to think about how we can eliminate some of these variables that may be problematic for someone who has had no prior experience with laser speckle or was trying to recreate one of our experiments. One of our early thoughts in designing an intuitive LSCI system for other research groups was how could we make the system a "turn-key" system. In theory, the user should be able to power on the system, engage the laser, and have the sample or sample plane be illuminated in an optimized fashion every time. We began to investigate the potential of using the microscope objective, which is commonly used in our groups' systems due to specific applications, to illuminate the sample as well as collect the scattered photons, which are then imaged by the detector. Such an illumination scheme would require that the illumination light share a portion of its beam path with the backscattered light. This means we need to ensure that there is no "cross-talk" between the two paths since they are of the same wavelength, and fundamentally we need some method of combining the two beam paths in the system.

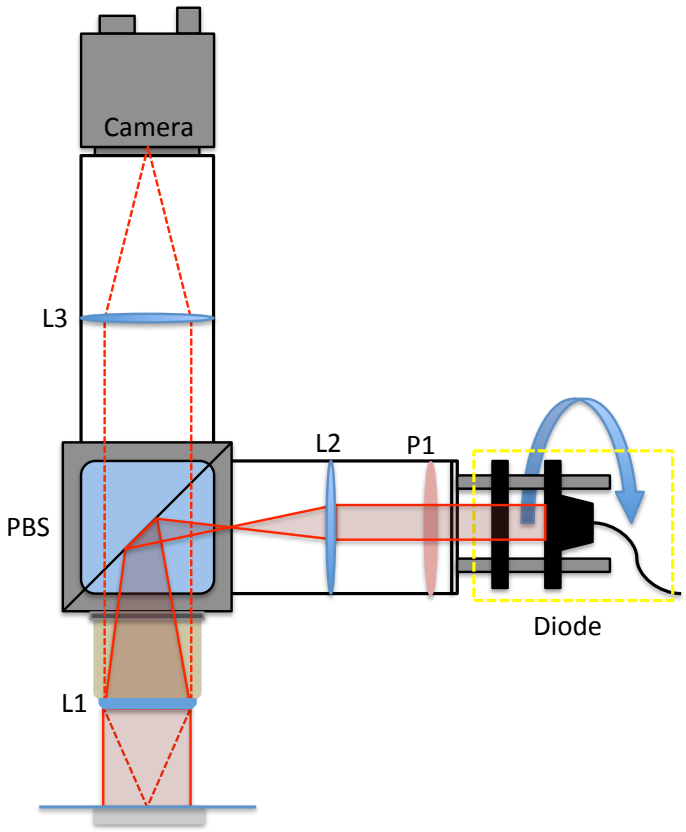

Figure 3: Schematic of LSCI set up with in-line illumination. L1 is the objective, and L2 and L3 are relay lenses. P1 is a linear polarizer mounted in a fixed position just after the diode that is mounted on a rotating cage mount (rotating components shown in yellow box).

We decided to use a polarizing beam splitter (PBS) to be the center of our system and therefore modify the polarization in the different arms of the system to enable the beams to share a common beam path without interacting with one another. Using this approach, we can integrate all the necessary components together in a basic cage-mounted system as shown in Figure 3. The PBS has two transmission axes that each pass one polarization component of light. If the illumination light is polarized along the transmission axes of the PBS, then the light will reflect 90 degrees towards the sample.

Laser diodes are inherently polarized which meant we needed to align the diode along the transmission axis of the PBS in order to allow the illumination light to be transmitted onto the sample. Once the illumination light exits the system through L1, the photons will enter the sample and undergo multiple scattering events. These scattering events will slightly change the polarization of the backscattered and back reflected light, which in turn will allow the components of the imaging light that are aligned with the other transmission axis of the PBS to pass through and reach the detector. The backscattered light that is passed by the PBS to the detector is cross-polarized with respect to the illumination light. This will affect our sampling by increasing our sensitivity to multiply scattered light that has undergone more depolarization. While the laser diodes are inherently polarized, the manufacturer does not label what the polarization of the output is in regards to the orientation of the physical diode.

Typically, in order to characterize the polarization, one would use a linear polarizer and rotate it to find out what orientation transmits or attenuates the most light. When the transmission axis of the polarizer is aligned with the polarization of the diode, most of the light will be transmitted. As the polarizer is rotated 90 degrees, the light will gradually be attenuated as the transmission axis is rotated out of phase. Shown in Figure 3, we placed a linear polarizer (P1) in the beam path and aligned it with the respective transmission axis of the PBS. Then we mounted the diode onto a rotating mount, which enabled the diode to be rotated about the axis of the beam path. We were not specifically interested with knowing the polarization of the diode, but rather making sure that the polarization of the diode was aligned with respect to the transmission axis of the PBS such that we maximize the throughput of our illuminating light. The rotation mount allows us to easily rotate the diode in order to determine what orientation most closely

aligns the polarization of the diode with the transmission axis of the PBS, but we found an added benefit of this design.

When performing an experiment with laser speckle imaging, if you have too much light incident on your sample such that you are saturating your camera, there are a few options that are used in practice to mitigate this issue. In a system with side illumination, you can first try to reposition the beam or to make it more divergent. Since we are operating within the constraints of the new in-line illumination, these quick fixes are not an option. One intuitive solution is to use a neutral density filter. This is a one-time fix that will evenly attenuate the light. Another potential solution is to decrease the drive current on the diode. Decreasing the drive current can compromise the coherence properties of the laser, which in turn will affect the speckle pattern. At this point, we decided to investigate the possibility of using the polarized elements in the illumination arm and the rotating mount to control the intensity of the illumination light without compromising the laser performance.

By first aligning the laser with both the polarizer and the PBS, we would transmit the majority of the light to the sample resulting in the largest possible intensity. As we rotate the diode from 0 to 360 degrees, we will start to reduce the intensity from 100% to 0% as dictated by Malus' Law shown below.

$$I = I_0 cos^2\theta \quad (2)$$

Malus' Law describes how plane polarized light is attenuated by a polarizer, where θ is the angle between the polarization axis of the light and the transmission axis of the polarizer. The intensity of the transmitted light is proportional to the to the square of the cosine between the transmission axis of polarizer and the orientation of the completely plane polarized light. In our setup, we actually are deploying two polarizers where the PBS acts as the "analyzer". This means that the linear polarizer acts to clean up

the diode's polarization, which naturally contains components of other polarizations. Now we have the ability to tune the intensity without compromising quality and more importantly, this method of control requires no technical expertise or optical experience.

Another benefit of the in-line illumination setup is that the system is robust and flexible which is important for the end user. The user can select whatever wavelength is best suited for the specific application as long as the filter and PBS are coated for the appropriate wavelength range. The other optical elements were selected to meet a couple specifications. For our purposes, L1 in Figure 3 is usually some sort of microscope objective. L1 can be substituted with any lens in reality but selection of this lens will determine L3 and L2. In the imaging arm, the relationship between the focal lengths of L1 to L3 will determine the magnification of the image. This in conjunction with the size of the detector in the camera will determine the maximum field of view. In the illumination arm, we initially selected L2 such that the beam exiting L1 was just slightly divergent. This relationship was initially thought to precisely follow the principles of a beam expander where placing the two lenses at a distance apart equivalent to the sum of their focal lengths will ensure a collimated input results in a collimated output. The expanding or shrinking of the beam is governed by the ratio of their focal lengths with respect to each other. We found that in the illumination arm, this relationship is tainted by some physical constraints of the system that are unknown to us, but we were able to achieve our desired goal by using a lens with a significantly longer focal length mounted on a sliding cage mount.

2.3 TIDIY

The main goal as previously mentioned was to create a do-it-yourself (DIY) speckle system that we can refer other research groups to who are interested in

performing speckle contrast imaging. This motivation to create a DIY setup led us to name the system TIDIY, or The In-line Do It Yourself speckle system. Once the system was designed, and the flexible pieces were identified along with a process for selection, we compiled a parts list of recommended components along with an instructional describing how to build and align the system. The instructional includes step-by-step instructions with visual aides to show how components interface with each other as well as procedurally how to align certain elements such as the linear polarizer. The last piece required for our modular, do-it-yourself speckle system is the software. Our lab has proprietary software enabling real-time speckle imaging amongst other features that have been added throughout the years. A compact, stripped down version is currently being compiled so that it can be distributed to other groups who are interested in constructing their own TIDIY systems. For maximum impact, the software must be de-bugged and tested to ensure that we can distribute the software in such a way where we do not have to provide technical support. This is in part due to the ongoing projects of members in our lab but in order to commercialize laser-speckle and drive its adoption, we need to remove the training wheels so to speak.

2.3.1 TIDIY Parts List

While the system was designed to be modular and allow for the researcher to interchange components such as the camera and diode, we settled on and employed an initial set of components which are shown in Figure 3, and will referenced by their labels in Figure 3 for this section. In the illumination arm, we selected a 658 nm diode laser (L658P040; λ=658nm, 40 mW, Ø5.6 mm, A Pin Code, Laser Diode Thorlabs Inc.) which was collimated using an aspheric lens (A220TM-B; f=11.0 mm, NA=0.26, Mounted Rochester Aspheric Lens, AR: 650-1050 nm Thorlabs Inc.) to correct for the inherent

astigmatism; both mounted on the rotating cage mount (CPR1; 30 mm Rotating Cage Segment Plate Thorlabs Inc.) shown in the yellow box on the right in Figure 3. Just after the rotating cage segment, we mounted a linear polarizer (LPNIRE100-B; Ø1" Linear Polarizer with N-BK7 Windows, 600-1100 nm Thorlabs Inc.) P1. Then a plano-convex relay lens (f=100mm Thorlabs Inc.), L2 was mounted on an adjustable cage mount between the polarizer and the polarizing beam splitter (CM1-PBS252; 30 mm Cage-Cube-Mounted Polarizing Beamsplitter Cube, 620-1000 nm Thorlabs Inc.), abbreviated PBS. A Nikon CFI Plan Achromat 10x Infinity Objective was mounted to the bottom of the PBS represented by L1, directly beneath the detector. The objective and the PBS are common to both the illumination and imaging arm of the system. Once backscattered light is collected through the objective and passes through the PBS, there is another 100 mm plano-convex relay lens (f=100mm Thorlabs Inc.), L3, placed approximately one focal length away from our camera (acA1300-60gmNIR; Basler Ace, GigE, 12 bit), which is a near infrared-enhanced camera. The entire system was mounted on a z-axis stage to allow the entire system to be adjusted as needed to get the sample in focus.

SECTION 2: STRUCTURED ILLUMINATION

Chapter 3: Single-Point Illumination

3.1 MOTIVATION

One inherent limitation of laser speckle imaging is its limited imaging depth. As previously mentioned, LSCI typically uses wide-field illumination with a red or near-infrared wavelength, to sample some volume of vasculature. The size of this volume has not been well characterized, but is determined by dynamic light scattering. In principle, as wide-field coherent light is exposed to the sample surface, photons enter the sample and begin to undergo multiple scattering events and in some cases, absorption events. In theory, every point in the sample is exposed to the same amount of photons, which undergo a symmetrical distribution of scattering events and then exit the sample. Through monte-carlo simulations, it has been shown with some accuracy that 95% of the LSCI signal comes from the top 700um of tissue[10]. These simulations did not account for the depolarization of light in tissue. In this scenario, the distribution of scattering events that result in ejected photons that reach the camera detector, only reach a depth of 700um. Some photons will sample deeper volumes, but not enough reach these depths, exit the sample surface, and reach the camera detector to create an appreciable signal. If we know that photons can sample deeper volumes, is it possible to deposit light into the tissue in such a manner that allows photons to interrogate these deeper volumes below the surface and reach still the detector?

One may first think that we should simply be able to increase the intensity of light and therefor increase the number of photons that are exposed to the sample, increasing the probability of photons reaching deeper depths and the distribution of scattering photons. In theory, this will physically increase the volume of tissue the photons

interrogate but only to an extent, and this increase may not even be detectable in our signal. An alternative we propose is based on the fundamental theory of noninvasive optical imaging, where we track photons deposited at a source as they migrate through a medium and are collected by a detector some lateral distance away shown below in Figure 4.

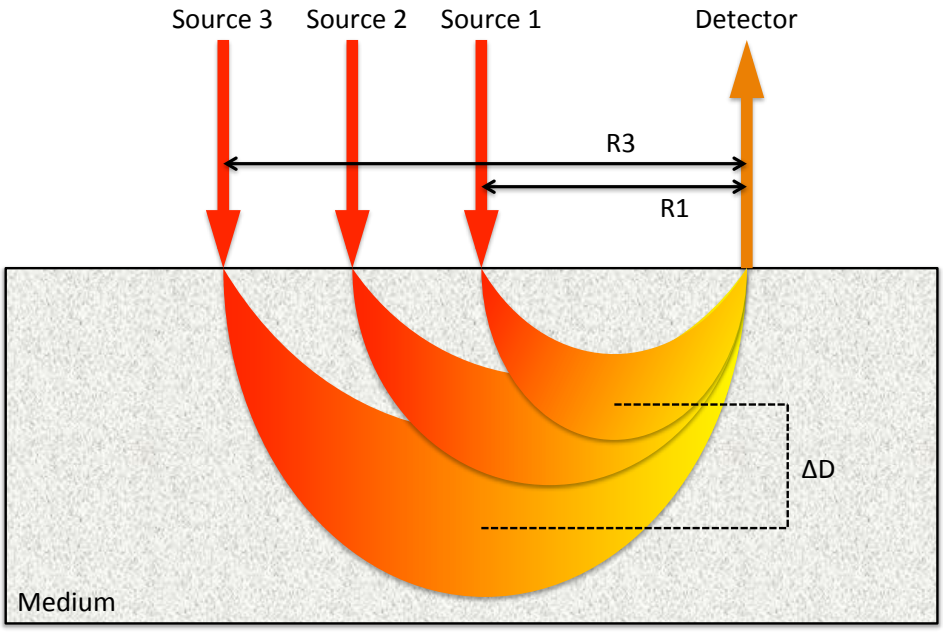

Figure 4: Theoretical photon trajectories for different source-detector combinations. R1 and R3 are radii representing the distance between the Detector and Source 1 and Source 3 respectively. For an increase in radii from R1 to R3, the sampling depth will increase by ΔD.

In order to characterize the photon trajectory, one must know the number of photons, or the intensity, deposited at the source and the optical properties of the sample that will determine the scattering and absorption events of photons. Here we propose an

alternative to wide-field illumination where we focus light to a point on the sample at different locations, represented by Source 1, 2, & 3 in Figure 4, and image with our detector some lateral distance away. Through proper characterization and testing, we propose that by modifying the distance between the source and detector, we can control the depth of interrogation. If this hypothesis holds true, we should be able to increase the source-detector separation from R1 to R3 as shown in Figure 4, and know that we have increased our sampling depth by some value ΔD.

3.2 METHODS

3.2.1 Instrumentation

In order to test this theory, we needed to design a setup that provided us control over as many parameters as possible. For this setup, the most important design criterion was focusing the light to a small spot on the sample, which increases the NA and in turn modifies propagation in the tissue, and having precise control over the location of the spot. While we previously demonstrated that in-line illumination removes the hassle of re-positioning the illumination beam every time, this advantage was inherent to the wide-field nature of the technique. While we could focus the illumination light in the in-line system, the light would be projected into the center of our camera's field of view, meaning we would have a source-detector separation of 0 mm. We could mount the relay lens shown in Figure 3 on an x y mount and move the beam path off axis to adjust the output out of the objective, but the NA of the objective would limit us as to how far we could move the spot.

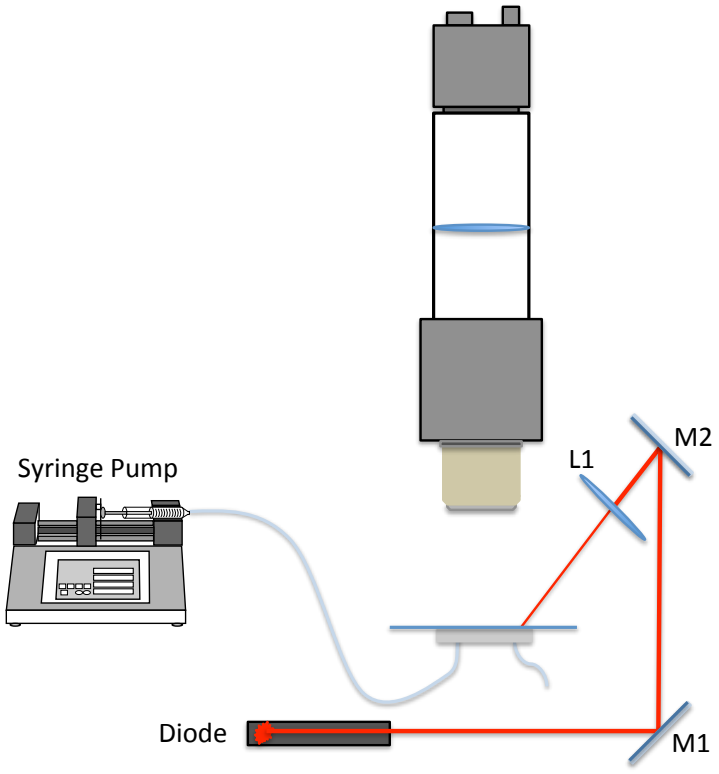

Figure 5: Schematic for single point experiments. Optics in the imaging arm are the same as in Figure 1. The 648 nm beam is steered using mirrors M1 and M2 and focused onto the sample via lens L1. Syringe pump connected to inlet line of microfluidic to supply flow.

Instead, we mounted the diode on an optical table and used the mirror arrangement shown in Figure 5 to guide and launch the beam into the sample. One priority in our design was to have the beam hit M2, and then launch perpendicularly into the sample. If the beam is not perpendicular to the sample plane, the photons will not sample the volume surrounding the spot in a symmetrical fashion. Rather, the volume sampled will be skewed in the direction the beam was angled upon interacting with the sample. For our setup, M2 needed to be as close to the objective as possible to achieve

this near 90° launch, but due to the physical size of the mirror, and the aperture of the objective, the beam was launched at a slight angle into the sample.

A diode laser (L658P040: 658 nm, 40 mW, Thorlabs Inc.) was selected as it was used in the previous setup and collimated to facilitate steering and positioning of the beam. The beam was steered using mirrors M1 and M2 (BBD1-E02: 1/2" Broadband Dielectric D-Shaped Mirror, 400 - 750 nm Thorlabs Inc.). Once the beam was directed towards the sample using M2, we focused the beam onto the sample using L1, a plano-convex lens (f=75mm, Thorlabs Inc.), which was mounted one focal length above the surface. For imaging, we used a NIR-enhanced Basler camera (acA1300-60gmNIR; Basler Ace, GigE, 12 bit) along with a 100 mm relay lens and 5x objective.

3.2.2 Experimental Design

Since we are trying to characterize the depth dependence of LSCI, we could not use a mouse because we can never know the true flow, location, or size of the range of vessels we would image in a craniotomy. Instead, we used a microfluidic channel, which allowed us to define the size, location, and flow while mimicking the optical properties of brain tissue.

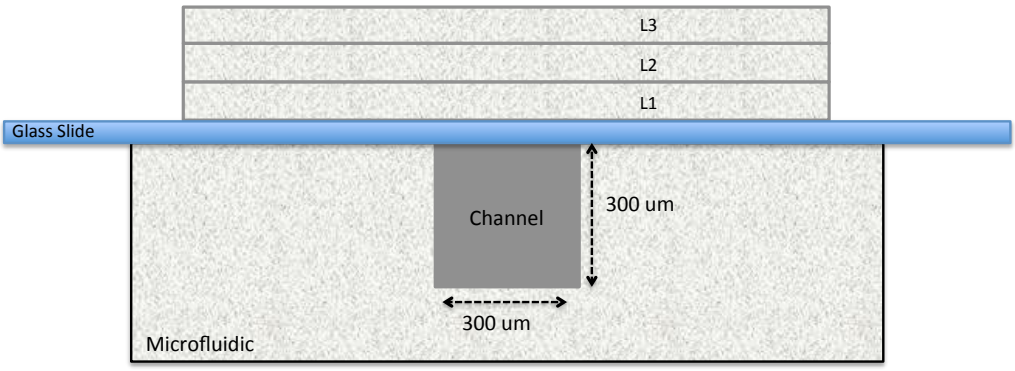

Figure 6: Cross-section of the microfluidic tissue phantom (straight channel) with added layers L1, L2, and L3. Layers are separated from the microfluidic by the glass microscope slide which is bonded to the bulk PDMS to seal the 300 μm x 300 μm channel.

We construct the microfluidic tissue-phantoms in-house using pre-fabricated aluminum molds that we design with different channel sizes and configurations. Channel sizes vary depending on what caliber vessels we are trying to mimic and can be designed with multiple branches to simulate capillary arrangements. For this experiment, we used a straight-channel with a height and width of 300 μm as shown above in Figure 6. To create the microfluidics, Dow Corning Sylgard® 184 PDMS (polydimethylsiloxane) was used in a 10:1 base-to-curing agent mixture by weight to create the bulk of the microfluidic. PDMS works well as a substitute for tissue as it has known optical properties, is solid when cured, and is flexible adding durability while allowing us to clean and reuse the phantoms. Titanium di Oxide (CAS 1317-80-2; TiO2; Sigma-Aldrich Inc., St. Louis, MO, USA) was added at 1.8 mg per 1 g of mixture to cause scattering in the PDMS to mimic the optical properties of tissue in the brain.

The PDMS and TiO_2 are first weighed and then mixed together for 15 minutes. Once the mixture is evenly mixed, it is centrifuged to remove any aggregates that could distort the optical properties of the phantom. The mixture is then poured over the aluminum mold in a petri dish and vacuumed to remove bubbles. Once the bubbles have been removed from the PDMS, the petri dish is placed in the oven to finish the curing process. After the PDMS has cured, the mold is removed, and the PDMS is cut to create a rectangular section that contains the channel on its top face. At this point, the channel itself has three sides composed of PDMS and requires bonding to a glass slide to seal the channel, and provide a window for imaging. Fusion of the glass slide to the microfluidic was done using oxygen plasma bonding.

For this experiment, we needed a way to simulate vessels located at different depths in the sample. This can be done for example by embedding glass capillaries within the PDMS during the fabrication process or bonding multiple pieces of PDMS together. These options and others, lack the ability to vary the depth of the channel without having to create a new microfluidic. Instead, we proposed to create thin layers of PDMS with TiO2 in the same ratio as described for the microfluidic, which we could then assemble in various combinations to simulate different depths. At first, we began by pouring small amounts of PDMS and TiO2 into petri dishes very slowly to see if we could create very thin layers around or less than a 1 mm thick. We struggled to accomplish this due to the viscosity of the PDMS which restricted the material from spreading out in the petri dish regardless of time, and once the material would reach the edges of the petri dish, the adhesion to the walls further restricted the minimum thickness we could generate. Instead, we elected to use an orbital shaker conventionally used for cell culturing. As the PDMS and TiO2 mixture was added to the petri dishes, the centrifugal force provided by the shaker would thin the material out despite the viscosity and in a relatively even

manner. This was then done in four petri dishes where the amounts of bulk material and the duration of shaking were varied to create an array of different thicknesses. After the PDMS in the four petri dishes had cured, rectangular sections the size of a glass microscope slide were cut across the center of each of the petri dishes. Because the mixture was added to the center of the petri dishes while they were shaking, the centrifugal force spread the mixture such that the thickness was most uniform directly around the center and would become noticeably thinner as you moved towards the edges. By cutting rectangular sections across the middle of each thin layer, we were able to stack layers on top of each other in such a manner that their original centers would align over the center of the channel. This allowed us to use the most consistent portion of the each of the original layers to simulate various depths in a reproducible manner. One corner of each layer was slightly clipped to allow us to consistently arrange the layers each time in order to prevent further variation.

Each layer had a unique thickness that was the result of various factors including the amount of bulk material poured and time placed on the shaker. To measure the thickness, a simple caliper was used and placed across the center of the layer, corresponding to the original center of the petri dish when the layers. In future experiments, the layers could be better characterized using optical coherence tomography (OCT), as the thickness is not actually uniform across the entire layer. For our purposes, this variation in thickness within each layer was negligible. The layers were arranged in combinations that provided us with a range of thickness; 0.6 mm, 1.1 mm, 1.3 mm, 2 mm, and 2.3 mm. We will refer to each experiment or trial by the absolute simulated depth, or combined thickness.

For any given experiment, there was a process for placement of the layers. First, layers were cleaned using isopropyl alcohol to remove any dust or debris and then air-

dried using the lab air supply. Layers were then gently placed one by one on top of the microfluidic ensuring the notched corners were aligned for consistency across experiments. A picture of the microfluidic setup is shown below in Figure 7 with three added layers to simulate a depth of 2 mm.

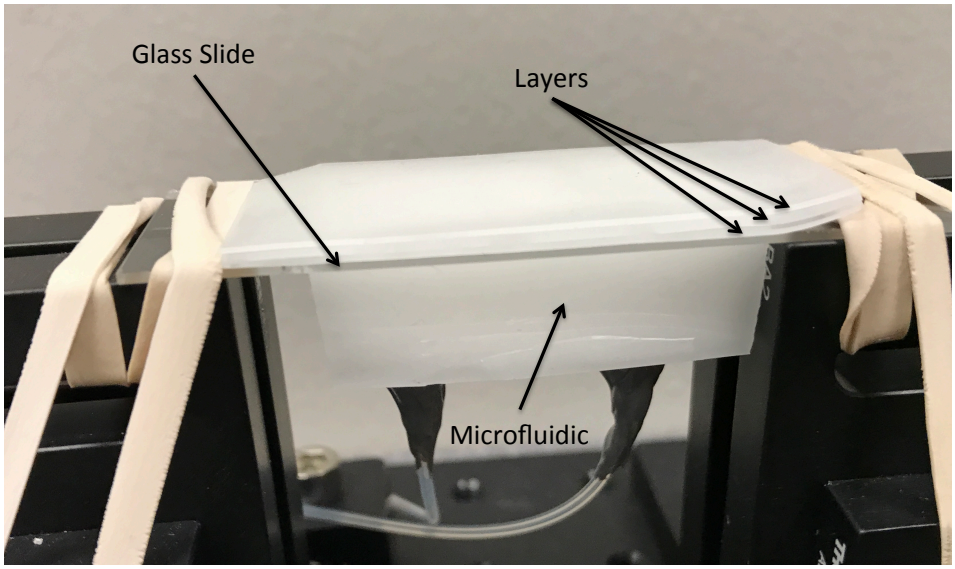

Figure 7: Photograph of microfluidic with static scattering layers placed on top to simulate a depth of 2 mm. The tubing that is entering and exiting the bottom of the microfluidic carries the microsphere formulation to the channel, which is covered by the scattering layers in this image. Edges of the glass slide that are not bonded to the microfluidic are secured to a mount using rubber bands to ensure the microfluidic does not move during experiments.

Once each layer had been placed on the microfluidic, a metal post was gently rolled across the top of the layer combination to ensure that there were no air pockets between layers and that the bottom-most layer was in complete contact with the microfluidic surface. Any air pockets between layers or between the layers and the

microfluidic would introduce an additional interface, which can result in unpredictable scattering. This scattering can affect how photons sample the channel in turn compromising results, so it is important to ensure no large air pockets are present.

To simulate blood flow within the microfluidic, we used a colloidal mixture of 1 μm diameter, polystyrene microspheres (5100A, Thermo Fisher Scientific Inc.) mixed with deionized water and a surfactant to mimic the scattering properties of blood. The mixture was formulated to achieve a $\mu_s' = 243\ cm^{-1}$. The mixture was sonicated and degassed in a glass vial before being loaded for each experiment to ensure the particles were fully suspended and no aggregates were present.

3.2.3 Illumination Scheme

The main goal of this experiment was to image the microfluidic channel with various layer combinations at three launch distances. The launch distance refers to the distance between the detector's field of view (FOV) and where the focused illumination light enters the sample as shown in Figure 4. In order to track the beam from one launch position to another, we had to manually adjust M2. This meant that if I wanted to reimage a previous location, I had to manually attempt to reposition the beam with no way of knowing if I was actually in the same location other than matching the histogram of the raw images in real time in the speckle software. This limitation led us to select three source locations at different distances based on ease of positioning. The first position as shown in Figure 8 was positioned to be located just outside of our field of view. Looking at the raw and speckle images on the computer, I could monitor the light levels which helped aid the visual eye in positioning the beam. Then, the third position was selected to be near the periphery of the glass slide as this was another obvious "landmark". The second position was then selected to be in-between Position 1 and Position 3. Obviously,

this illumination scheme is not ideal as it is impossible to perfectly reposition the beam but we believed we should be able to exploit a trend, if one existed, using careful planning and manipulation of the few tunable variables we had control of.

Flow in the microfluidic was set at a constant 50 µl/sec for all experiments. A constant flow program was selected for all the experiments, as we are primarily concerned with sensing flow at different depths and source locations as opposed to sensing changes in flow.

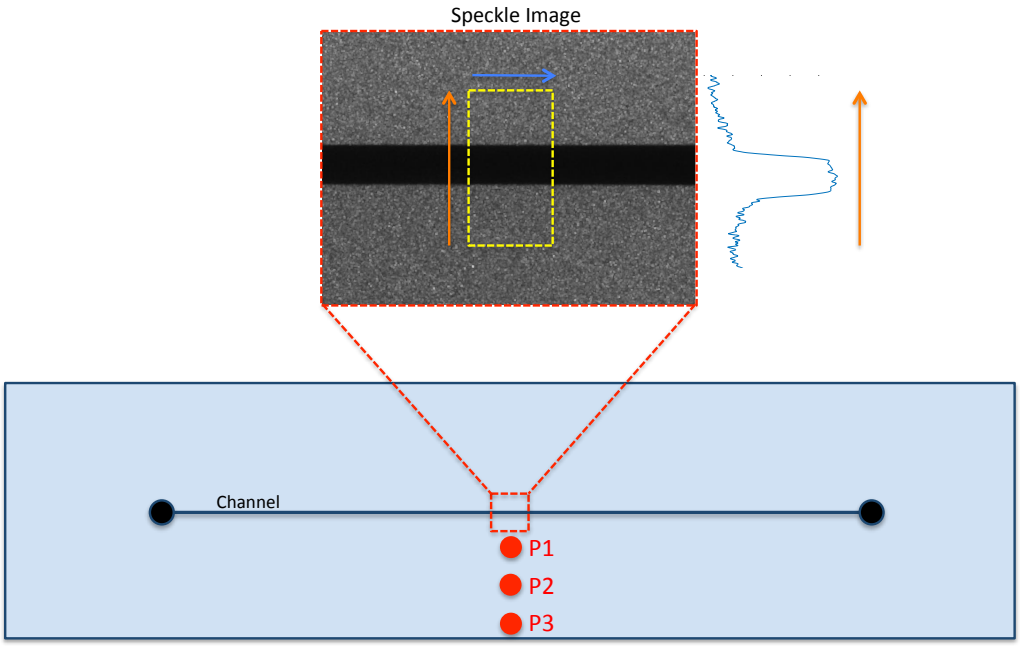

Figure 8: Top-down view of experimental setup for single point, straight microfluidic experiments with source positions P1, P2, and P3 shown. Red, dashed box represents the camera FOV. Within the FOV, data was extracted from the yellow ROI where the blue line is the dimension averaged across and the orange line represents the line profile for which the averaged values in the ROI are plotted, shown to the right of the speckle image.

In order to measure the flow in each layer and source location combination, we selected a region of interest (ROI) as shown in the yellow box above in Figure 8. The ROI was centered across the channel at approximately the center of field of view. First, we averaged the ROI taken from 80 consecutive frames. We then averaged the SC values across the ROI shown by the blue arrow in Figure 8. This ensured we were adequately sampling the SC values and did not capture random fluctuations that may occur at one specific time point. Once we averaged the SC values across the ROI, we then plotted the values across the channel shown by the orange line. When plotted, the x-axis corresponds to the position across the cross-section of the ROI, whereas the y-axis corresponds to the SC values averaged across the ROI.

3.3 Results & Discussion

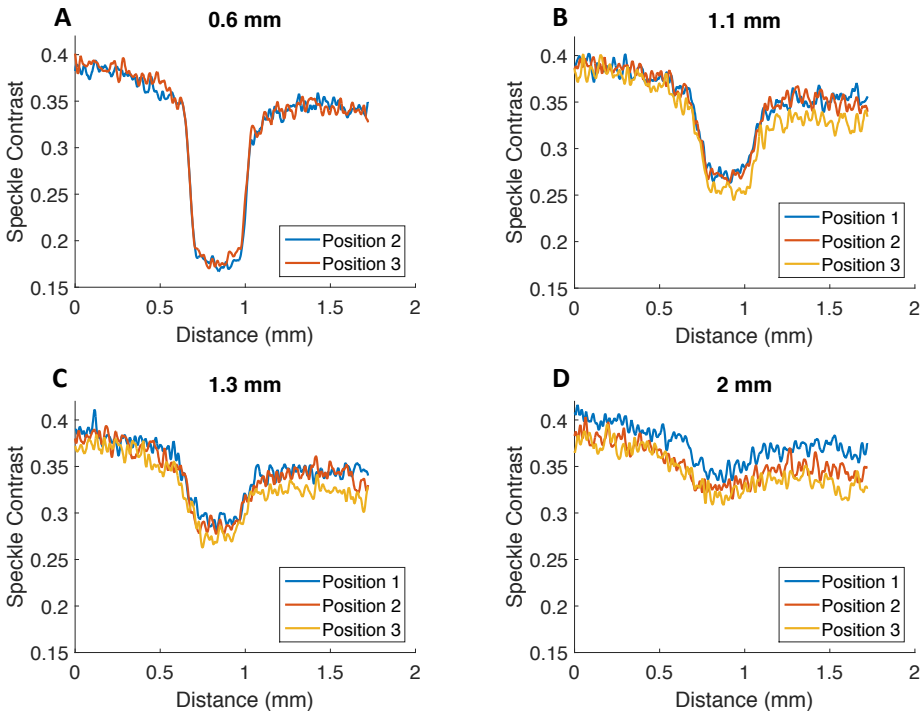

Figure 9: Profiles taken across the straight microfluidic with single point illumination at simulated depths of 0.6 mm (A), 1.1 mm (B), 1.3 mm (C), and 2 mm (D).

Shown in Figure 9 are the plots of speckle contrast values at four simulated depths, measured using three source locations as previously described. In Figure 9A, Position 1 was not plotted as the proximity of the source location in conjunction with such a thin, 0.6 mm static scattering layer resulted in excessive saturation. The plots for Position 2 and Position 3 in Figure 9A are nearly identical, which suggests that at this simulated depth, there are enough photons sampling the channel at each source location such that the flow is being consistently detected. The x-axis is plotted such that 0 mm

corresponds to the point that is closest to the source location. We can definitively see in Figure 9A-C, that the SC values from the static regions of the microfluidic are less on the side of the microfluidic that is farthest from the source location. In theory, the SC values should not change in the static regions but in practice they do, as there is a natural gradient of light beginning at the source location and radially decreasing in photon density. This is consistent with the fundamental theory of noninvasive optical imaging previously described in 3.1. With that being said, in Figure 9B-D, the SC values inside the channel, and on the side opposite of the source, are appreciably changed in the presence of the flow. This confirms that focused light from our source out of frame is sampling the channel, exiting through the added scattering layers, and then reaching our detector. In Figure 9D, this dip, which corresponds with flow in the channel, becomes significantly less pronounced. While one can argue we are still detecting the channel to some extent hinting at a small "dip", we are beginning to detect the limits of this technique given our setup at depths of approximately 2 mm. In Figure 9C, there is seemingly a change in SC values with each source location, especially within the channel. This would follow along with what we expect to be true, that as you increase your source detector separation, the photon trajectory in the sample will vary which ultimately changes how deep you are sampling. We hope that at a specified depth, as we increase the source detector separation, we will begin to tailor our sampling volume to best interrogate the channel and accurately measure flow information. With that being said, we are not sure whether the photon trajectories of each source detector configuration are sampling part of the channel, static regions above or below the sample, or combinations of both. Further characterization of how the sampling volume and measured speckle contrast change as a function of source detector separation is required.

Chapter 4: Single Point Illumination with Branched Microfluidic

4.1 Motivation

After the first series of experiments, we felt as if we were headed down the right path but needed to improve our experimental design and data collection in order to better understand the relationship between sampling volume and source detector separation. One option we considered based off some prior literature, was to have two channels either at different depths or locations within a phantom such that we could collect information from both while we altered the layer thickness or the source location[11]. Theoretically, by collecting two sets of data, one on each channel, we could modify the depth and source location such that we could interpret trends between data collected from both channels since we would know the physical separation between them and the optical properties of the medium in between. Ultimately, we decided to test a branched microfluidic that had just been fabricated for other tests in our lab at the time. Our hope was that having a spatially, slightly more complex channel geometry would provide more understanding as to how source detector separation governs sampling.

4.2 Methods

4.2.1 Instrumentation

The experimental setup was the same as described in section 3.2.1.

4.2.2 Experimental Design

The branched microfluidic used for this experiment was fabricated using the same materials and methods described previously in section 3.2.2. The channel in this microfluidic was designed as a straight channel that branches into two channels and then recombines creating a hexagonal shape as shown below in Figure 10.

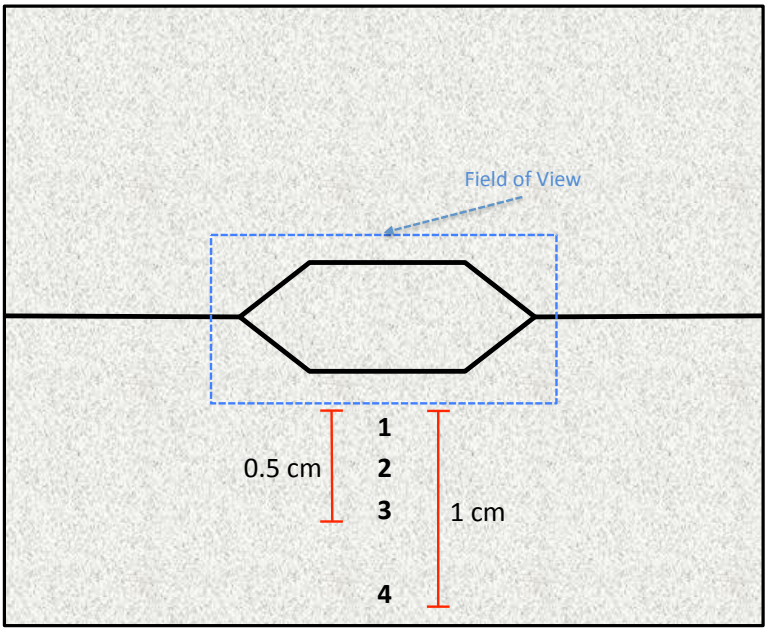

Figure 10: Top-down view of branched microfluidic with no added layers. blue-dashed line shows the camera FOV. Source locations 1, 2, and 3 are placed within the first 5 mm outside of the FOV and source location 4 is approximately 10 mm from the FOV.

Each branch is 300 μm x 300 μm in size, which is the same size as the straight microfluidic used in the first experiment. Since the branches are symmetrical and the same size, we know that the flow in each branch is the same.

The thin layers of PDMS used to simulate various depths were the same as described in section 3.2.2.

The microsphere solution for this experiment was modified due to unexpected formation of aggregates during testing. As described in section 3.2.2, the mixture was originally formulated to achieve a μ_s' = 243 cm^{-1}. During our initial tests in the branched microfluidic at various simulated depths, we began noticing some changes unexpected changes in relative flow. When we removed the layers, it was evident that microspheres

were beginning to aggregate and form clumps visible in the speckle contrast image in regions where the channel wall changed direction. Initially, we thought this due to the fact that we were occasionally using microsphere formulations that were up to a week old. Our typical "quick fixes" we attempted were to increase the overall speed of flow as well as manually squeezing the syringe loaded in the syringe pump to induce a brief period of rapid, turbulent flow to dislodge any aggregates. Manually purging the line with the syringe would often clear a couple of the visible aggregates but required a large amount of the loaded formulation to be expelled and we often could see aggregates reform quickly after. While we typically can reuse formulations a couple days later without problems, for publishable data, it is recommended that you make a fresh microsphere mixture. We then began to test mixtures that were synthesized on the day of or were at most one day old, but still had issues with aggregate formation. Next, we tried to increase the duration of sonication and degassing performed before synthesizing the mixture as well as once the mixture was made but prior to loading it into the syringe. Despite all our efforts, we still had issues with aggregation formation, which led us to ultimately decrease the microsphere concentration achieve a $\mu_s' = 197$ cm^{-1}. This scattering coefficient is less than that of whole blood but is still a relatively good model of scattering for our purposes.

If you are also using some method of simulating various depths, you may not be able to detect the clumps without removing the static scattering medium or using a precise flow sensor. In our experiments, clumps often weren't detected until we were well into a set of experiments such that we had to remove all the layers to check the flow in the channel. In doing this, we change the placement of the layers which required us to recollect data.

4.2.3 Illumination Scheme

Similar to the experiment performed on the straight channel, the goal of this experiment was to measure the flow in the microfluidic at various simulated depths across a range of source locations. In this experiment, we tested a fourth source location as shown in Figure 10 because the microfluidic had more bulk material between the channel and edge of the microfluidic.

We were still limited by manually having to track the laser to each source location, so we used another very basic illumination scheme using identifiable "landmarks" to position each source location. Position 1 was still located just outside the field of view as shown above in Figure 10, and such that saturation was minimized with no layers added. Position 4 was then placed at the periphery of the glass slide but such that there was still PDMS below the glass. The method in which the microfluidics are cut after the PDMS cures, results in sections that are typically narrower than the glass microscope slides which means when we bond them together, the glass slide extends past the edges of the PDMS. When positioning the beam at the farthest source location, it is important that there is PDMS below the glass at that location or else we introduce a glass air interface that can affect our sampling. Position 3 was then selected to be halfway between Position 1 and Position 4. Lastly, Position 2 was placed in between Position 1 and Position 3. While tracking the beam between the source locations, I was able to develop a general feel for how some degree of manual manipulation of the mirror translated to a physical displacement of the beam on the microfluidic. When coupled with the information provided in real time by the live speckle and raw images, I could reposition the beam in the various locations pretty well for each simulated depth. This illumination scheme was not ideal and had many issues regarding variability and reproducibility.

4.3 Results & Discussion

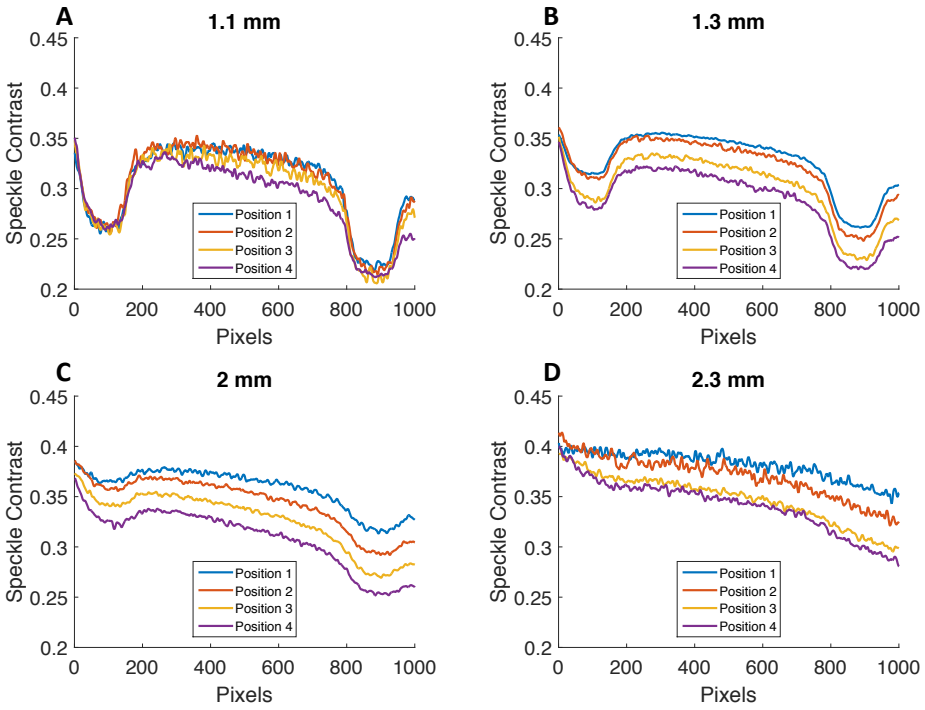

Figure 11: Profiles taken across the branched microfluidic with single point illumination at simulated depths of 1.1 mm (A), 1.3 mm (B), 2 mm (C), and 2.3 mm (D).

In Figure 11A, we can see that each source location is detecting the same apparent flow. We know therefor that the photon trajectory at each source location can adequately sample a channel at a depth of 1.1 mm. We also know that Position 4, which is approximately a total of 10-12 mm from the second channel, is adequately sampling the channel and detecting a very similar flow as the other source locations. It is important to highlight that in Figure 11A, the SC values of each source location within the channel are nearly identical, even at the second channel, yet between the channels, as we move closer to the second channel, the plots begin to deviate. We know that the space between the

channels is a static medium, so the fact that the SC values begin to deviate in Figure 11A and then reconverge in the presence of flow in the second channel may provide insight into how the photons are truly sampling the channel. In Figure 11B and C, we start to detect some stratification of detected flow between source locations. In both plots, Position 1 has the largest SC value, which then gets slightly smaller as you increase the source-detector separation. The signal is degrading as the simulated depth is increased but this technique still performs better than full field illumination in detecting flow in a submerged vessel. There are two points to note here. We must consider the possibility that due to the photon trajectory and number of photons traveling between the source and detector, the photon trajectory depicted in Figure 4 may be sampling different parts of channel. In Position 4, the photons could be largely passing underneath the channel with just a small fraction sampling the lower portion of the channel. There is no way to truly know if this is the case, especially as all photons must interact with static scattering medium between the channel and the detector. The other consideration is that for illumination schemes at simulated depths where the trends between each source location are consistent but decreasing in magnitude, such as in Figure 11C, there is some relation governing the decrease in magnitude and therefor must be some way of eventually incorporating a scaling factor based on the source detector relation we hope to uncover. We can also see in Figure 11C that the dips that correspond to each channel are much less pronounced across all of the positions when compared to Figure 11B. Likely, this is due to the increased layer thickness that will cause further scattering of photons that sample the channel prior to exiting the top of the static layers. Again, we do not know if all or any of the photon trajectories at each source location completely or partially detect the channel and with what level of accuracy. Interesting to note is how much the quality of the signal decreases as we move from Figure 11C to Figure 11D which is only a

difference of 0.3 mm. This means that given our setup, at a depth of 2.3 mm one cannot say with any confidence that we are sampling the channel. This may indicate we are reaching our maximum source detector separation for the given channel and experimental parameters such as the intensity of the light. This setup still only utilizes single focused beam, which means there is a natural gradient as photons propagate radially from the source location. As the density of photons continually declines as source detector separation increases, our measured flow will likely decline as well. In Figure 12B below, we can see that in the raw image at Position 4, there is seemingly no light or insufficient light reaching the detector.

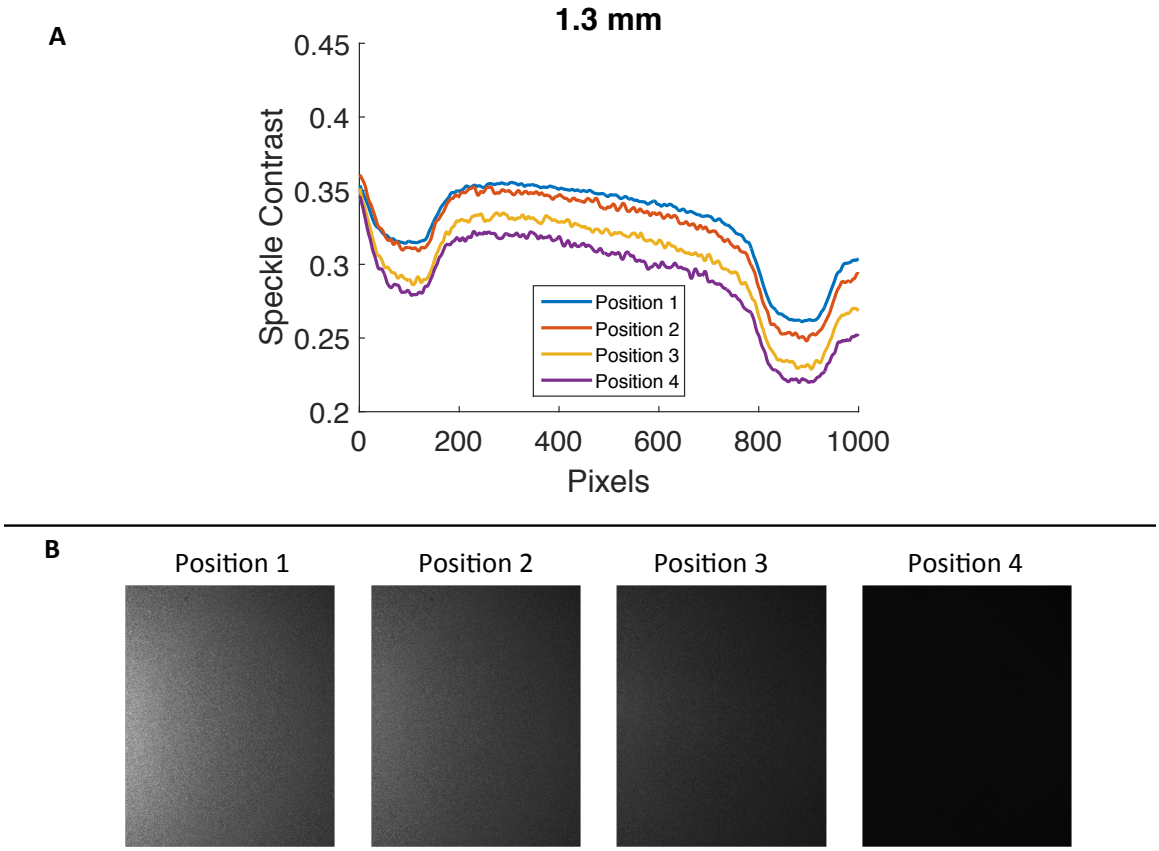

Figure 12: (A) Profiles taken across the branched microfluidic at four source locations at a simulated depth of 1.3 mm (B) Raw image from each of the source locations.

We can see that in Figure 12A, Position 4 seems to sample the channel sufficiently well. This makes it difficult to know if we are truly reaching the limit of this relationship between source detector separation and sampling depth depicted in Figure 11D. Not only do we need more data from a greater sampling of source locations and layer thicknesses, but we also need to explore how increasing the number of photons that reach a vessel at a specific depth changes the apparent flow.

Chapter 5: Two-Point Illumination with Branched Microfluidic

5.1 MOTIVATION

In considering our current setup and the necessary next steps, we wanted to investigate some illumination schemes that consisted of more than one source. It would be interesting to know how the addition of an identical source, placed the same distance on the other side would increase the photons sampling the channel and the measured flow. The second source would need to be identical to the first in terms of intensity as well as geometry and height associated with the launch angle to ensure the combined setup is symmetrical. Having a symmetrical illumination scheme with a second source allows us to analyze our results to some extent ignoring the effects of the photon gradient that occurs with a single source. We know we would have theoretically doubled the amount of light sampling the channel by applying an even but opposite photon gradient through the addition of a second source. If achieved, we could potentially write off the effects of the natural gradient from each individual source experienced with a non-full field technique.

5.2 METHODS

5.2.1 Instrumentation

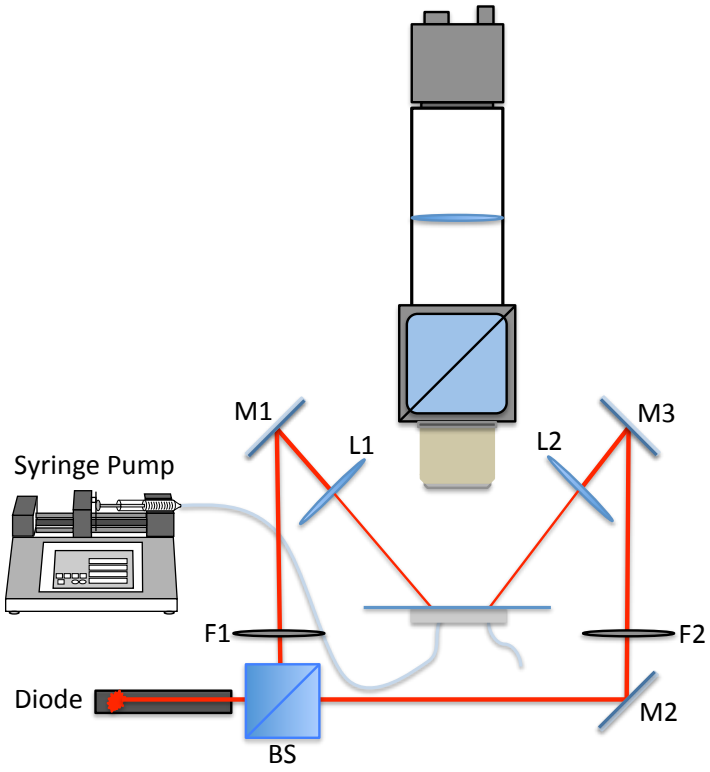

Figure 13: Schematic for double point illumination experiments. Optics in the imaging arm are the same as in Figure 1. The 648 nm beam is evenly split 50/50 by the BS and then both beams are directed to the sample using M1, M2, and M3. Lenses L1 and L2 were used to focus the beam to the sample while neutral density filters F1 and F2 were used to balance the intensities of the focused beam. Syringe pump connected to inlet line of microfluidic to supply flow.

The experimental setup was the same setup used in the single source illumination scheme with a couple modifications. To achieve two source locations with the same intensity, we used a simple 50/50 beam splitter (BS). A BS ensures that the original beam is evenly divided into two beams of the same intensity. This was more feasible than using

two separate, identical diodes that could vary slightly in performance despite being potentially easier to maneuver and position on the sample. After the BS, we wanted to make the new beam path as similar to the beam path common to the earlier setup, shown in Figure 13 reflecting off of M2, so a focusing lens of the same power was added at the same location after reflecting off of M1 which was placed approximately at the same position as M3 on the other side of the microfluidic. While M1 was positioned such that it is in the same location with respect to the sample as M3, the actual angle at which the light is incident on the sample and location will vary to some extent which limits our ability to definitively draw any conclusions from our results. Despite slight differences in the angle of the beam at each source location as a result of the mirrors and focusing lenses, two neutral density filter combinations were added to the beam paths to intensity match the sources.

5.2.2 Experimental Design

The thin layers of PDMS used to simulate various depths were the same as described in section 3.2.2.

The microfluidic was the same as described in section 3.2.2 and the microsphere solution used in this experiment was the same as described in section 4.2.2.

5.2.3 Illumination Scheme

As previously described, the main goal of this setup was to use a symmetrical, multi-source illumination scheme to confirm that the apparent flow is different depending on simulated depth such that we can ignore the effects of the photon gradient from a single focused source. For simplicity, we decided upon two possible locations for each source on either side of the channel, located at equivalent distances as shown below in Figure 14.

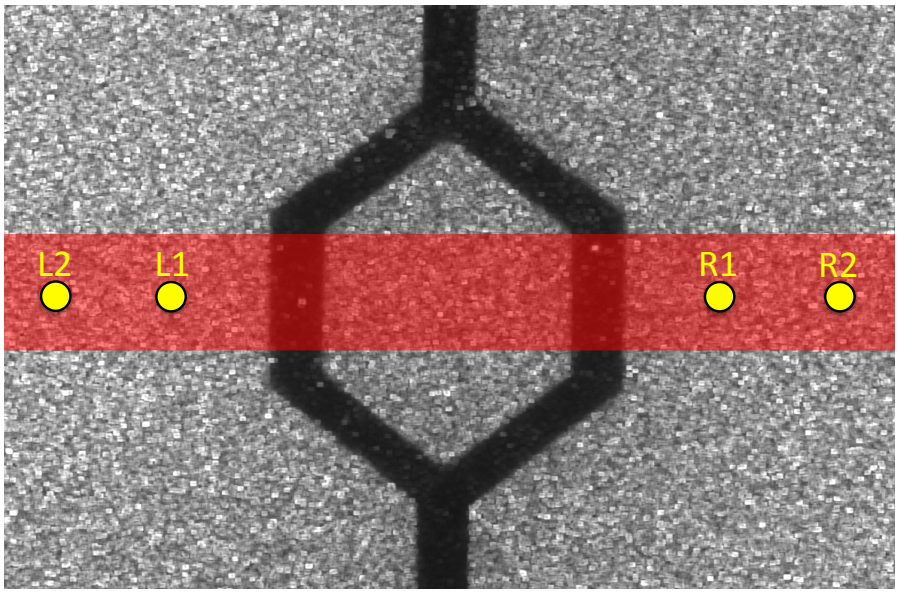

Figure 14: Camera FOV for experiments using the branched microfluidic. Source locations for double point experiments L1, L2, R1, and R2 are shown in yellow (source locations were located outside the FOV and shown here for illustrative purposes). The ROI in red was averaged across its width and then the profile across both channels was plotted.

Figure 14 serves only as a visual aid to understand the illumination scheme as all source locations in experiments up to and including this one were located outside of the detector field of view, which is shown here in a processed SC image. In actuality, Figure 8 shows where the source locations are actually located in relation to the camera's field of view. The sets of source locations were chosen such that the farther set, L2 and R2, were twice as far from the respective channels as L1 and R1. This was done for simplicity so that when interpreting any potential trends, moving from one source location to another would change the relative source detector separation by a factor of two in either direction. In the earlier experiments, determining the exact effect on

measured flow moving between sequential source locations spaced a few millimeters apart, along with the inconsistency of tracking the beams manually with the mirrors, is very difficult. Given our illumination scheme with source location sets, for each trial our approach was to start with a symmetrical source combination, then move only one of the source locations to create an uneven illumination scheme, and separately measure each source location used in the final set independently. This was done for each of the various layer combinations used to simulate different vessel depths similar to the previous experiments. Since the first illumination scheme is a symmetrical set, we hoped that movement of one source location of the set to create an uneven scheme could tell us how moving the one source location closer or farther away changes the measured flow. Once we have measured the two sets of source locations, measuring each component independently could potentially lend some insight into how the sampling volume is being modified.

5.3 Results and Discussion

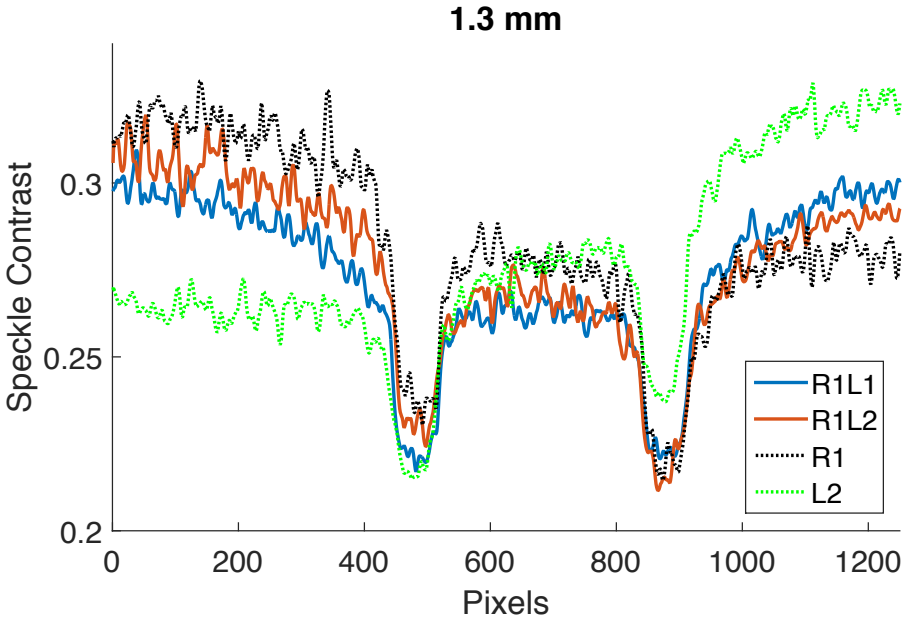

Figure 15: Plot of double point illumination scheme and components across the branched microfluidic at a simulated depth of 1.3 mm.

In Figure 15, all of the plots are inverted with respect to the physical microfluidic. This means that when looking at contributions to the measured flow from one source location, if that source location was on the right side of the microfluidic, the gradient of light will be shown decaying from left to right. In the earlier experiments, we noticed that when comparing the apparent flow at two sequential source locations, the magnitude was lower at the farther of the two locations. In Figure 15, as we move the position of the left source location from L1 to L2, the measured flow in the channel closest to the source locations on the left side decreases as described, while the measured flow in the channel farther from the source locations increases. Comparing the red line against the blue line in the plot, we can see this. One potential explanation is that as we move from L1 to L2,

the photon trajectory is sampling deeper such that more photons are traveling through or beneath the nearest channel and collectively doing a better job at sampling the farther channel. This is a nice theoretical for why there is an increase in apparent flow in one channel and a decrease in the other as we've come to sort of expect, but further characterization for a greater sampling of source locations must be done. The dotted plots in Figure 15 that represent the individual source locations, support the expected trend but must be taken with a grain of salt as they ultimately only confirm that at least between the two channels, when the source location is at L1 or R1, the difference in apparent flow in the two channels is seemingly smaller than when the source location is at L2 or R2. Ultimately, we know we are slowly learning how to test a trend that is repeatable, and reversible but requires a more thorough and extensive characterization of how source location and depth affect the measured flow.

Chapter 6: DMD

6.1 MOTIVATION

In order to achieve a more extensive characterization of the relationship between source location and depth, we needed to create a setup that would allow us to rapidly cycle between illumination schemes and easily modulate their complexity. The setups used for the previous experiments are limited in their complexity, and require a lot of work to modify them to achieve a different illumination scheme. We knew that after the first couple iterations, we would likely move towards symmetrical illumination schemes that would consist of a grid of sources in either a 2x2 or 3x3 arrangement. The illumination scheme described in 5.2.3 required placing two mirrors as close as possible to the objective to attempt to achieve a 90° launch into the sample. This becomes very difficult to accomplish due to the physical size of the mirrors and the elements required to mount and hold the mirror in the position. You would also need to be able to split the source beam or deploy multiple lasers and steer the beams to reach the mirrors placed at the objective. Nevertheless, a better method for creating the illumination schemes was required that was not as tedious or inconsistent.

To do this, we decided to use a digital micromirror display (DMD), to spatially modulate our illumination beam. A DMD is a small chip that contains hundreds of thousands of individually controlled mirrors that enable light modulation. Each mirror can be individually turned on or off which corresponds to a change in mirror angle. When light is exposed to the DMD surface, only the mirrors that are turned on, will direct light down the optical path. The other mirrors in the off state will throw the rest of the light away from the optical axis such that it does not contribute to the projected image. Individual control of this complex mirror array allows series of mirrors to be engaged to

project precise patterns. For our purposes, we envisioned we could integrate a DMD into our in-line speckle system described in Chapter 2, where mirrors in the on state would project light down the in-line, optical axis shown on the right in Figure 3. Using the in-line design, instead of a full-field illumination, the DMD would shape the illumination beam and send structured light through the PBS and objective to the sample. If we needed to change to a more complex, or just different illumination scheme, we would simply have tell the DMD what pattern we want, and the mirror array would be appropriately modified to project the desired pattern. This design would eliminate the physical optical elements and time required to split the beam and physically steer each beam to the sample required for a given illumination scheme.

6.2 METHODS

6.2.1 Instrumentation

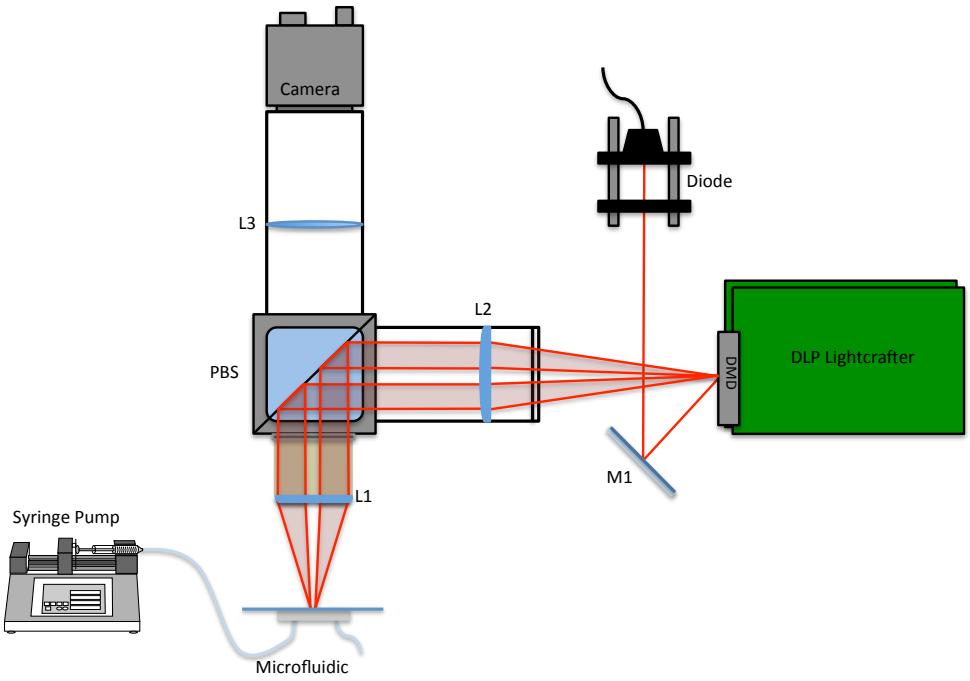

Figure 16: Schematic of the DMD-based illumination system. Optics in the imaging arm are the same as in Figure 3 (Section 2.4). A 648 nm beam is directed onto the face of the DMD using M1. The structured light is then collected using L2 and relayed through the objective L1 using the PBS. A syringe pump was connected to the microfluidic inlet to supply flow.

The experimental setup for this DMD-based system was designed for rapid modulation and cycling of illumination schemes, in a repeatable manner that ensured the sample was being interrogated the same way during any experiment. This idea is similar to what was described in the conception of the TIDIY system, where in-line illumination made interrogation of the sample more robust. With full field, side illumination, the beam

and the nature in which it propagates, diverges, and is exposed to the sample varies between experiments and in some cases between trials. We navigated this issue using the in-line illumination, which used the objective to guide the illumination light to the sample. For the DMD-based system, we wanted to use the same in-line approach to remove the variability in a setup like described in 5.2.3. Since the sample or region of interest is positioned directly under the center of the objective, it seemed intuitive that using the objective as the final lens for our illumination optics would ensure that we could achieve symmetrical illumination schemes using the DMD.

The DMD is sold by Texas Instruments as part of a DLP® Lightcrafter™ Evaluation Module (DLPC3000), which is an all-inclusive, bistable light modulator. Included in the system are a light engine, process and control boards, and the DMD itself, which is 7.62 mm x 4.28 mm. The process and control boards allow for USB connection of the module to the software interface in order to program and control the DMD pattern display. The light engine is a light source that is powered by the driver board and then exposed to the DMD itself to create the desired pattern. Light reflected off of the DMD is collected using internal optics and then projected out of the system. For our purposes, we are only interested in the using the raw DMD, and the process and control boards required to control and modulate the DMD. We sought to use a higher power, coherent light source at a red-shifted wavelength to ultimately enhance our ability to image deeper with speckle. Since the DMD is packaged with the pre-selected light engine and internal optics, the system had to be disassembled in order to remove the unnecessary components. Texas Instruments has a video that details how to properly disassemble and remove the unwanted components.

Once the DMD was stripped of the unnecessary components, we mounted the DMD as shown in Figure 16 with the face of the DMD exposed to the right surface of the

PBS. This was done so when light was reflected off of the “on” mirrors, the light would be directed down the optical path towards the PBS to achieve in-line illumination as previously described for the TIDIY system. Mirrors on the face of the DMD in the off state would direct light away from L2 shown in Figure 16.

To illuminate the face of the DMD, we selected a diode laser (HL6385DG: λ=642nm, 150 mW, Ø5.6 mm, H Pin Code, Laser Diode Thorlabs Inc.) and used a D-shaped mirror (BBD05-E02: 1/2" Broadband Dielectric D-Shaped Mirror, 400 - 750 nm Thorlabs Inc.) to direct the beam to the DMD shown as M1 in Figure 16. In order for the light reflected off of the DMD to travel down the desired optical path, light must be exposed to the DMD surface at approximately 24°. This specific angle is determined by the range of motion of the mirrors which totals to about 24° considering each mirror is at either ±10-12° depending on if it is in the on or off states. To achieve this precise angle, M1 had to be placed as close as possible to the optical path without obstructing the illumination light. This is why a D-shaped mirror was used, as a normal 1” circular mirror would extend into the beam path.

Once light is exposed on the face of the DMD and modulated as desired, the structured light is collected by L2 in Figure 16, which is a plano-convex relay lens (f=75mm Thorlabs Inc.). While the light is collimated until it is exposed to the DMD, the DMD acts as projector causing the light reflected off the surface to diverge until reaching the image plane. L2 collects the modulated light allowing us to direct it through the PBS and L1. The lenses L1 and L2 were selected to achieve a magnification of 0.394, which ensures the DMD is entirely projected into the camera FOV. The illumination light was not polarized using a linear polarizer and therefor the amount of illumination light transmitted through the PBS is determined by the polarization of the light diffracted off

the DMD face. The PBS, imaging optics, camera, and L1 are the same elements as described in section 3.2.1.

Once all of the elements have been positioned as shown in Figure 16, there is a significant amount of aligning that must be done to ultimately ensure that the face of the DMD is properly imaged to the image plane. Each mirror on the DMD array corresponds to a pixel in the image to be displayed, in our case an illumination scheme. If the optics in the system are not appropriately selected to map the DMD face to the sample plane, then it will be impossible to create even, symmetrical illumination schemes. The first step in aligning the system is properly positioning M1 as previously described to achieve an angle of about 24° with respect to the in-line optical path. Once this is done, the live image in the speckle software was used to roughly see how evenly light was illuminating the sample. Assuming the DMD and laser are aligned properly and the DMD face is imaged to the onto the sample plane, the intensity of the light across the sample should be uniform. If the alignment is imperfect, M1 can be adjusted roughly using the post-mount system or finely using the knobs on the mirror mount to change how the beam is reflected onto the DMD. This process can be very tedious so the DMD was placed on a micrometer operated tip, tilt, and rotation stage to offer some precise control of another element in the system. It is a fine balance between ensuring the face of the DMD is appropriately positioned with respect to the PBS and beam path, and making sure that the beam is precisely directed onto the DMD face. Control over multiple variables such as the mirror and DMD position can help to facilitate this process.

6.2.2 Experimental Design

The microfluidic was the same as described in section 3.2.2 and the microsphere solution used in this experiment was the same as described in section 4.2.2.

Due to time constraints, we were only able to test the DMD-based illumination schemes on the raw microfluidic without any scattering layers.

6.2.3 Illumination Scheme

The illumination scheme for the first set of experiments was designed to be consistent with the prior experiments to see if we could confirm the trends we detected using a more robust setup. We decided to use a two-source setup similar to that described in Chapter 5, which could then be easily modified to a single source setup in Chapter 3 and 4. One more complex scheme, consisting of a 2x2 grid of sources, shown in blue in Figure 17 was designed to investigate illumination schemes that were symmetrical in two dimensions as opposed to just one.

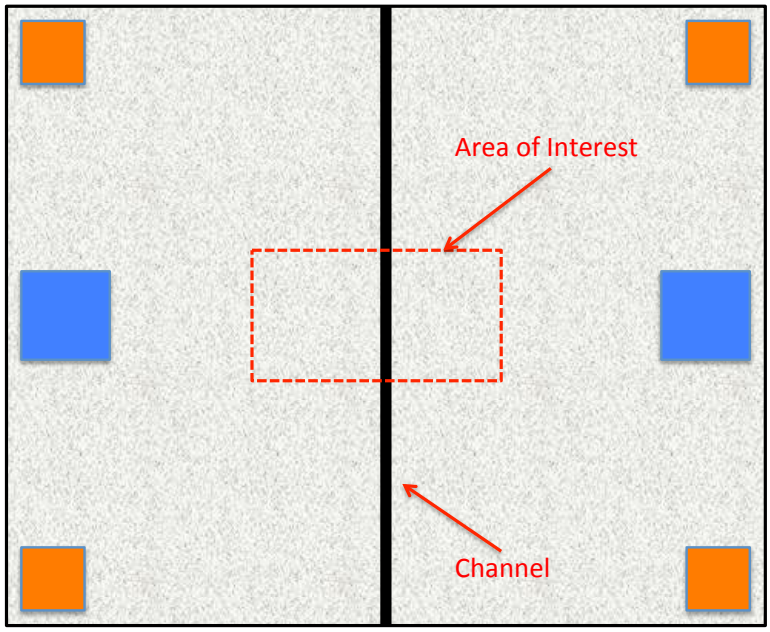

Figure 17: Illustration of the DMD-based illumination schemes projected within the camera FOV. Shown in orange are the four 50 μW, intensity matched ROI's which comprise the 2x2 grid illumination scheme. Shown in blue are the two 0.2 mW, intensity matched ROI's used to recreate the two point illumination scheme. The ROI in blue on the left was used for the single point illumination scheme.

In designing the illumination schemes, we thought it was important to for the sources in the symmetrical schemes to be intensity matched. Since the symmetrical illumination schemes are centered on the middle of the camera's FOV, intensity matching the source locations ensures each one evenly contributes to the sampling of the channel. In theory, if the system is perfectly aligned, when all the mirrors are on the intensity should be evenly spread across the camera's FOV. To draw each illumination scheme, you just need to tell the DMD how large to make each ROI shown in Figure 17 and the

DMD will engage the same number of mirrors corresponding to each source location. In reality, our system was not perfectly aligned so intensity matching the source locations, especially in the 2x2 illumination scheme, was done manually. Control over the DMD had been previously integrated into our speckle software that allows us to control and monitor our illumination scheme from one central location. Each ROI was drawn to be the same size, then the DMD was turned on and the intensity was measured using a photodiode. The intensities were matched to the first ROI that was drawn. Each ROI was initially drawn to match the size of the first ROI but if the intensity was lower, then the ROI was redrawn slightly bigger until the intensity was matched. Making the ROI slightly bigger engages more mirrors on the DMD, which will increase the amount of light reflected down the optical path effectively increasing the intensity. For consistency between the two point illumination scheme and the single point illumination scheme, the two ROI's for the two point illumination scheme were first drawn and intensity matched, and then one ROI was turned off creating a single point illumination scheme that had exactly half of the light.

6.3 Results and Discussion

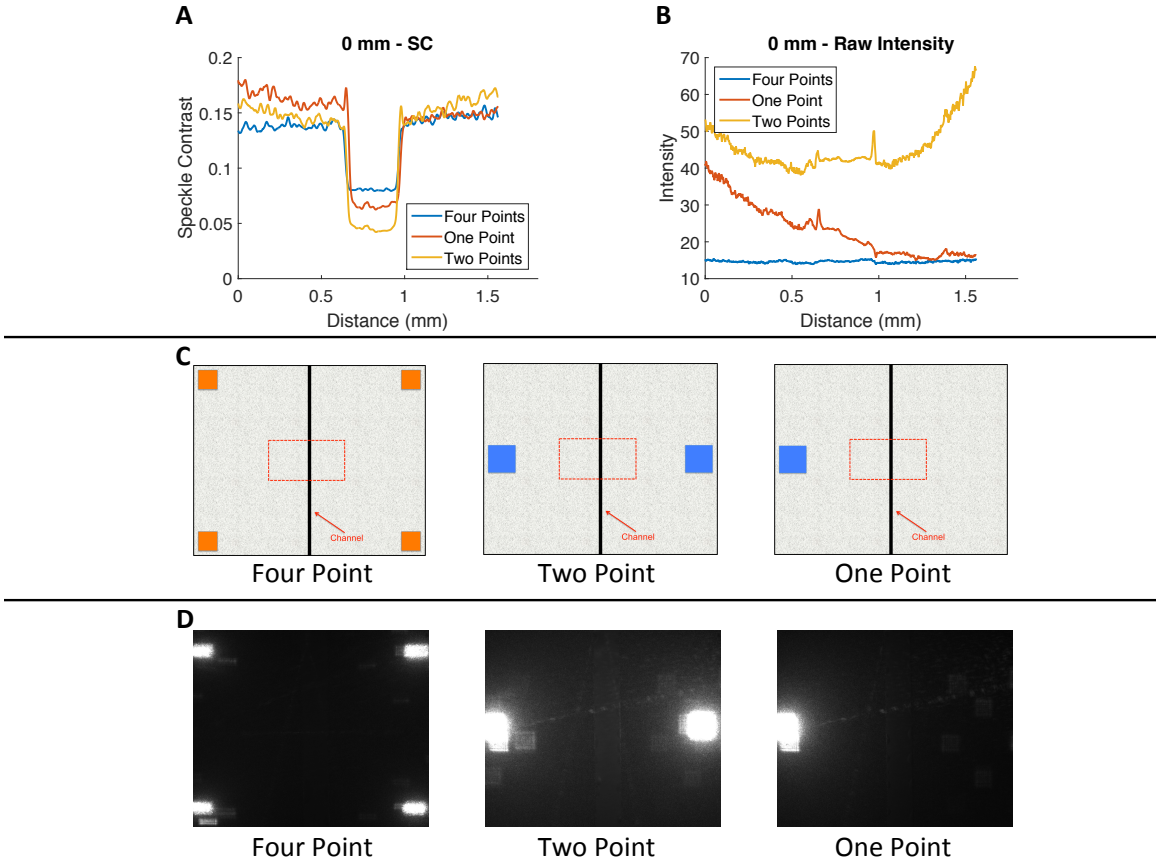

Figure 18: (A) Plots of speckle contrast values across the straight microfluidic channel with no static scattering layers for the DMD-based illumination schemes. (B) Plots of the raw intensity for each of the plots in Figure 18A. (C) Schematic of each DMD-based illumination scheme drawn within the speckle software. (D) Raw images of each DMD-based illumination scheme.

In Figure 18A, are the cross-sections through the microfluidic using the DMD-based illumination schemes. It is important to note that in the four-point grid scheme and the two-point grid scheme, the intensity at each source location was matched for consistency. In the four-point illumination scheme, each point had an intensity of approximately 50 μW, totaling to about 0.2 mW which was slightly less than half of the total intensity used for the two-point illumination scheme. We can see in Figure 18A that

SC measured in the channel using the four-point illumination scheme was significantly less than the SC measured using the two-point illumination scheme. The two-point illumination scheme reported a faster relative flow. The single-point illumination scheme had an intensity of about 0.2 mW, similar to the total intensity for the four-point illumination scheme, yet the relative flow is greater than that detected using the four-point illumination scheme despite having near equal absolute intensities. This led us to postulate whether each illumination scheme was sampling the channel differently or if the stratification in relative flow measured was due to the light levels at the detector. In Figure 18B, we plotted the same ROI used to measure SC in Figure 18A but plotted the absolute intensity measured by the detector. We can see in Figure 18B that the light levels were lowest for the four-point illumination scheme and highest for the two-point illumination scheme. The light levels at the detector for the single-point illumination scheme was greater than that of the four-point illumination scheme because all the light was deposited at one source location as opposed to four equally spaced sources even though the absolute intensities were nearly the same.

Moving forward, it seems that it is important to match the intensity at the detector as opposed to matching the source intensities. This would ensure that no matter the illumination scheme, the same amount of light reaches the detector. We need to figure out the relationship between SC and intensity variations. It is evident that under the same flow conditions and experimental parameters that increasing the intensity will increase SC even though theoretically, SC should be independent of intensity. While a lower intensity will decrease the mean SC value, the standard deviation should change proportionately as well, which is clearly not the case.

Chapter 7: Conclusions

In this thesis, a new method of illumination for speckle imaging, in-line illumination, was presented which offers significant advantages over conventional side-illumination. Not only is in-line illumination more robust, which eliminates variations in different side illumination configurations, but using a polarizer and a PBS, users can freely control the intensity of the illumination light without changing parameters that may affect laser performance.

In-line illumination then led to the development of TIDIY, a turnkey, DIY speckle system that can be distributed to other groups interested in performing LSCI. This system provides researchers the flexibility to deploy components for any application and includes a step-by-step instructional detailing how to assemble and align the system.

Creation of a robust, in-line illumination scheme ensured that researchers could illuminate a sample in a repeatable, "turnkey" fashion. Geared with this knowledge, we questioned if we could modify how we distribute light in the sample to obtain further depth-resolved information. By changing source detector separation at different simulated depths, it was evident that it is possible to sample vessels located under up to 2 mm of static scattering layers. More complex microfluidic geometries were implemented to exploit the photon gradient in a point-source detector arrangement.

A two-point illumination scheme was then tested that discovered symmetrical illumination schemes can increase the information collected from the vessel by increasing the number of photons that interact with the vessel, travel through the static scattering layers, and then reach the detector. Further testing of more source-detector distances along with spatially complex illumination schemes, led to the development of a DMD-based LSCI system.

This DMD-based system enables rapid cycling of illumination schemes in turn eliminating the need for physical maneuvering of components of each illumination scheme to the sample. Preliminary results confirmed that a DMD-based setup can deliver sufficient light to the sample in a structured fashion, but also called into question the relationship between intensity and SC. Results suggest that moving forward, illumination schemes should be designed to match the intensity of light in the detector space as opposed to in the sample space.

References

1. Dirnagl, U., Kaplan, B., Jacewicz, M. & Pulsinelli, W. Continuous measurement of cerebral cortical blood flow by laser-Doppler flowmetry in a rat stroke model. *J Cereb Blood Flow Metab* **9,** 589–596 (1989).
2. Lauritzen, M. & Fabricius, M. Real time laser-Doppler perfusion imaging of cortical spreading depression in rat neocortex. *Neuroreport* **6,** 1271–1273 (1995).
3. Ances, B. M., Greenberg, J. H. & Detre, J. a. Laser doppler imaging of activation-flow coupling in the rat somatosensory cortex. *Neuroimage* **10,** 716–23 (1999).
4. Fercher, A. F. & Briers, J. D. Flow visualization by means of single-exposure speckle photography. *Opt. Commun.* **37,** 326–330 (1981).
5. Dunn, a K., Bolay, H., Moskowitz, M. a & Boas, D. a. Dynamic imaging of cerebral blood flow using laser speckle. *J. Cereb. Blood Flow Metab.* **21,** 195–201 (2001).
6. Ruth, B. Measuring the steady-state value and the dynamics of the skin blood flow using the non-contact laser speckle method. *Med. Eng. Phys.* **16,** 105–111 (1994).
7. Yaoeda, K. *et al*. Measurement of microcirculation in optic nerve head by laser speckle flowgraphy in normal volunteers. *Am. J. Ophthalmol.* **130,** 606–610 (2000).
8. Stern, M. D. In vivo evaluation of microcirculation by coherent light scattering. *Nature* **254,** 56–8 (1975).
9. Briers, J. D. & Webster, S. Laser speckle contrast analysis (LASCA): a nonscanning, full-field technique for monitoring capillary blood flow. *J. Biomed. Opt.* **1,** 174 (1996).
10. Parthasarathy, A. B. & Bharadwaj, A. Quantitative cerebral blood flow measurement with Multi Exposure Speckle Imaging. (2010).
11. Mazhar, A. *et al*. Laser speckle imaging in the spatial frequency domain. *Biomed. Opt. Express* **2,** 1553–1563 (2011).